Dalton Transactions

ROYAL SOCIETY OF CHEMISTRY

FRONTIER

View Article Online
View Journal

Cite this: DOI: 10.1039/d0dt02798g

Current status and future prospects of metal–organic frameworks at the interface of dye-sensitized solar cells

Ruhollah Khajavian, Masoud Mirzaei * and Hanie Alizadeh

Received 10th August 2020,
Accepted 1st September 2020

DOI: 10.1039/d0dt02798g

rsc.li/dalton

The implementation of metal–organic frameworks (MOFs) as an integral part of dye-sensitized solar cells has received increasing attention over the past decade. Much effort has been devoted to improving the performance of these cells by optimizing the photosensitizer, photoanode, and counter electrode. This Frontier Article provides a snapshot of the recent advances in each of these three major directions achieved *via* MOF implementation.

Introduction

Dye-sensitized solar cells (DSSCs), a class of low-cost photoelectrochemical cells with a facile manufacturing technology, have become one of the most studied classes of photovoltaic devices.[1] The system consists of a wide bandgap semiconductor, a light absorber molecule (dye), and a redox mediator all assembled between working and counter electrodes. A sensitizing dye is immobilized onto the surface of the semiconductor (TiO_2 or ZnO) *via* anchoring groups. Upon the absorption of light, photoexcited electrons transfer from the LUMO level of the dye to the conduction band of the semiconductor. Then, the redox couple (usually iodide/triiodide) reduces the oxidized dye back to its neutral state and transports the positive charge to the counter electrode (Pt).

After the initial reports in the mid-2000s,[2,3] the capability of metal–organic frameworks (MOFs) in producing charge separation has been a matter of intense studies. The highly ordered networked structures of MOFs are composed of organic ligands (also called linkers) that link metal ions or metal oxide clusters (Secondary Building Units: SBUs) to each other. Although still controversial,[4] the nanoporous and modular character of MOFs paved the way for them to be considered, implemented and fix a number of traditional problems associated with classic dyes. For example, by utilizing the organized and open framework of a MOF, a higher density of dye molecules can be incorporated, preventing dye aggregation, poor electrolyte access, and reduced charge transfer.[5,6] In addition, higher efficiencies in photon capturing are possible when using MOFs as cosensitizers.[7] To this end, MOF implementation has shown promising results; yet, there remain challenges that need to be addressed before these functional materials become fully applicable in DSSCs.

Due to the infinite number of combinations between metal ions and ligands as well as ordered porous structures and diverse topologies, MOF-related studies have formed a highly dynamic multidisciplinary research field. They are traditionally used for catalysis,[8,9] gas storage,[10] and drug delivery,[11] where their high surface area and permanent porosity play important roles.[12] A survey of the literature shows that there has been growing interest among the scientific community for utilizing MOFs as an integral part of photovoltaic cells during the past decade and abbreviated terms "MOFSC"[13] and "MSSC"[14] were appeared in the literatures published in 2016 and 2017, respectively.[15–18] MOFs could be used as various components in a DSSC device (Fig. 1). This can be achieved either by replacing the existing components with a suitable MOF or using a MOF-derived material. The former case includes using MOFs as the light-harvesting sensitizer or as host for other materials (guest@MOF concept). The idea of using MOFs for passing or controlling the current in a cell is the most challenging part of work, as MOFs exhibit insulating behavior.[19] In the latter case, MOFs are used as precursors for the synthesis of functional elements with specific properties. This Frontier Article tries to highlight the most recent advances in each direction presented in Fig. 1 through a systematic approach, but the reader can be informed of other studies with more general approaches elsewhere.[20–22]

MOFs as sensitizer

In general, the photoconversion efficiencies observed with MOF-sensitized solar cells are still low (Table 1). Nevertheless, the possible diversity in size, functionality, *etc.* of both the metal nodes and linkers gives hope for future progress in this area.

Department of Chemistry, Faculty of Science, Ferdowsi University of Mashhad, Mashhad 9177948974, Iran. E-mail: mirzaeesh@um.ac.ir

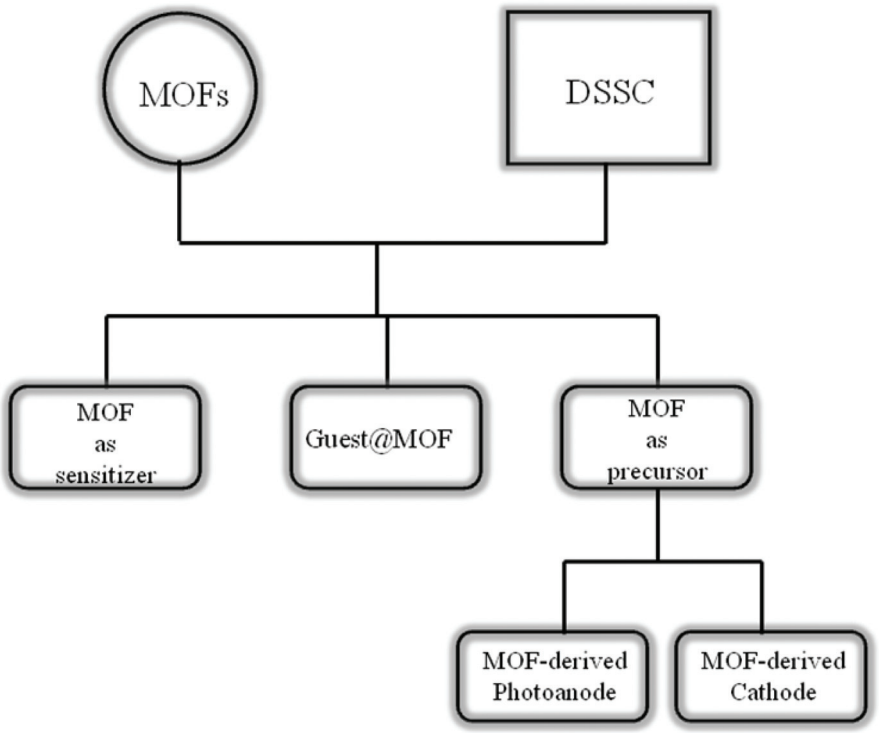

Fig. 1 A schematic representation of the different roles of metal–organic frameworks in a dye-sensitized solar cell.

The prerequisite for utilizing a material as a dye in a DSSC is its ability to capture photons within the entire visible spectrum. When it comes to MOFs, this could be achieved through their ability to encapsulate multiple light absorbers and locking them into a stable crystalline structure. Porphyrin-containing linkers were among the first-studied photosensitizers for MOF-based cells due to their intense absorption bands in the red part of the visible region.[14,29] The energy and charge transfer mechanisms are also well studied in porphyrin-based MOFs.[72–75] Liu *et al.* utilized porphyrin-containing linkers in combination with closed-shell zinc ions to minimize exciton quenching. The work also suggested that introduction of Zn or Pd centres increases the bandgap from 1.58 eV for free-base porphyrins to 1.88 and 1.94 eV for zinc- and palladium-metallated linkers, respectively.[76] Tuning the optical and electronic properties of MOFs has been a subject of intensive research thus far and several studies have demonstrated that band structure adjustment could be achieved by varying the composition of the building blocks.[77,78] One strategy for increasing the light-harvesting efficiency is to increase the conjugation length of the ligand.[79] It was shown that the introduction of long alkyl chains into MIL-125-NHR (R: methyl to *n*-heptyl) led to a gradual decrease in the optical bandgap. Remarkably, substituents with stronger electron-donating ability exhibited higher stability and longer lifetime of the charge separated state (Fig. 2).[80] Wöll *et al.* pointed out the importance of introducing electron-donating DPA groups onto the *meso* positions in a Zn porphyrin SURMOF to improve the solar light absorption and photocurrent generation characteristics of the cell.[81]

Another approach to bandgap engineering is through changing the composition of the metallic node. DFT calculations and experimental observations revealed a reduction in bandgap with an increase in the exchange of Zr ions with Ti in UiO-66.[82] Very recently, Eddaoudi, Gascon, and coworkers used a similar approach to synthesize a highly visible-light-responsive MOF. During photocatalytic experiments (HER), it was found that the combination of H_4TBAPy, as a photon antenna, with Ti-oxo clusters produces a system in which electrons are highly mobile along the Ti–O–Ti–O chains and holes are localized on the linker.[83] Another promising solution is to introduce sensitizers as chromophoric sites into the MOF scaffold. A beautiful example is the work of Morris *et al.*, who doped $Ru^{II}(bpy)_2L$ (L = 2,2′-bipyridine-5,5′-dicarboxylic acid) into UiO-67 through the coordination of 2,2′-bipyridine-5,5′-dicarboxylate with zirconium nodes within the MOF scaffold.[13,84] More recently, transition metal ions (Co, Ni, and Cu) were incorporated into amine-functionalized MIL-125 through coordination with the $-NH_2$ group. This study showed a significant improvement in the solar light absorption property of pristine MOF *via* the contribution of d–d transitions. A metal-ion dependency was also observed in the charge carrier separation rates.[85] Another method for inducing light harvesting in MOFs and boosting photocurrents is through sensitization with QDs.[86] Beside photovoltaic characteristics,[34–36] it has been shown that the confinement of QDs (perovskite) inside MOF pores has a synergistic effect on the stability of the perovskite and MOF film.[34,87,88]

Table 1 Summary of the various applications of MOFs in DSSCs[a]

Photosensitizer	J_{sc} (mA cm^{-2})	V_{oc} (V)	FF (%)	PCE (%)	Anode	Cathode	Ref.
NH_2-UiO-66	0.00639 ± 0.0001	0.87516 ± 0.005	53.16 ± 5	0.003 ± 0.001	TiO_2	Au	23
NH_2-UiO-66(Zr/Ti-35%)	0.06535 ± 0.0001	0.88562 ± 0.005	59.52 ± 5	0.034 ± 0.001	TiO_2	Au	23
$Cu_2(bdc)_2(bpy)$	0.064	0.21	33.2	0.004	TiO_2	Pt	24
$Cu_3(btc)_2$	0.0285 ± 0.0085	0.416 ± 0.0275	47.5 ± 13	0.005 ± 0.0007	TiO_2 + DHBA	Pt	25
$Cu_3(btc)_2$	0.05	0.37	41	0.008	TiO_2	Pt	26
$Ru_3(btc)_2$	0.33	0.48	39	0.06	TiO_2	Pt	27
$Al_2(bdc)_3$	0.02335	0.266	33.84	—	TiO_2	Au	28
PPF-4	0.0085 ± 0.00099	0.515±.0065	52.1 ± 0.66	0.0023 ± 0.0003	TiO_2	Pt	14
[100]-PPF-11	4.20 ± 0.50	0.47 ± 0.002	41 ± 4	0.82 ± 0.05	ZnO	Pt	29
$[InK(ox)_2(H_2O)_4]_n$	3.84	0.61	64	1.5	TiO_2	Pt	7
$[In_{0.5}K(3\text{-qlc})_2Cl_{1.5}(H_2O)_{0.5}]_{2n}$	4.31	0.62	59	1.59	TiO_2	Pt	7
Eu-MOF	20	0.449	44	2.3	TiO_2 + graphene	Pt	30
MOF-5	0.209	0.52	58	—	TiO_2	Pt	3
Ru-DCBPY-UiO-67	0.446 ± 0.097	0.480 ± 0.019	55 ± 4	0.123 ± 0.021	TiO_2	Pt	13
RuDCBPY-ZrMOF	0.564 ± 0.129	0.482 ± 0.035	47 ± 4	0.125 ± 0.038	TiO_2	Pt	13
Co-DAPV	4.92	0.67	57	2.1	TiO_2	Au	31
Co-bdc	0.04	0.23	29	0.003	TiO_2	Pt	32
Co-ndc	0.04	0.24	29	0.003	TiO_2	Pt	32
$I_2@Cu_2(bdc)_2(bpy)$	0.323	0.54	40.7	0.071	TiO_2	Pt	24
$I_2@Cu_3(btc)_2$	1.25	0.49	43	0.26	TiO_2	Pt	26
$I_2@Cu_3(btc)_2$	1.95	0.48	51	0.46	TiO_2 + MWCNT	Pt	33
$I_2@Ru_3(btc)_2$	2.56	0.63	63	1.22	TiO_2	Pt	27
I_2@Co-bdc	2.13	0.62	62	0.96	TiO_2	Pt	32
I_2@Co-ndc	2.56	0.63	63	1.12	TiO_2	Pt	32
$DMB@Al_2(bdc)_3$	0.0362	0.361	40.46	—	TiO_2	Au	28
C_{60}@[100]-PPF-11	0.67 ± 0.30	0.335 ± 0.032	59 ± 5	0.13 ± 0.04	ZnO	Pt	29
Perovskite@MOF-525	23.04 ± 1.0	0.93 ± 0.02	60 ± 3	12 ± 0.5	TiO_2	Ag	34
CdTe@Eu-MOF	28.45	0.349	30.5	3.02	TiO_2	Pt	35
CdTe@NTU-9	23.19	486	28.5	3.20	TiO_2	Pt	36

MOF-derived photoanode	J_{sc} (mA cm^{-2})	V_{oc} (V)	FF (%)	PCE (%)	Dye	Morphology	Ref.
MIL-125	13.99	0.768	67	7.2	N719	Octahedron	37
MIL-125	17.27	0.81	58.18	8.10	Cu_2ZnSnS_4 + N719	Cube-like	38
MIL-125	19.1	0.66	55	7.1	N719	Bipyramid	39
MIL-125	17.72	0.60	77.88	8.96	MoS_2	Cylinder	40
MIL-125	16.5	0.74	61	7.45	N719	Mesoporous	41
ZIF-8	9.13 ± 0.23	0.667 ± 0.008	55.4 ± 0.4	3.37 ± 0.06	N719	Rhombic dodecahedron	42
MOF-5	7.95 ± 0.17	0.646 ± 0.006	68 ± 1	3.49 ± 0.04	N719	Parallelepipeds	43
Zn-MOF-1	—	—	—	0.15	N719	Elliptical microparticles	44
Zn-MOF-2	—	—	—	0.14	N719	Elliptical microparticles	44

MOF-derived cathode	J_{sc} (mA cm^{-2})	V_{oc} (V)	FF (%)	PCE (%)	Electrolyte	Composition	Ref.
PIZA-1	17.26 ± 0.10	0.76 ± 0.01	69.42 ± 1.05	9.11 ± 0.09	I^-/I_3^-	$CoS_{1.097}$@N-doped carbon	45
ZIF-67	14.7	0.784	71	8.1	I^-/I_3^-	CoS	46
ZIF-67	15.87 ± 0.10	0.72 ± 0.01	71.1 ± 0.98	8.18 ± 0.08	I^-/I_3^-	Co@N-doped CNT	47
ZIF-67	18.3	0.76	65	9.04	I^-/I_3^-	CoNi@CNT-carbon	48
ZIF-67	18.86	0.72	67	9.06	I^-/I_3^-	$CoSe_2$/N-doped carbon	49
ZIF-67	16	0.71	67	7.58	I^-/I_3^-	CoSe@N-doped carbon	50
ZIF-67	17.89 ± 0.05	0.787 ± 0.003	64	9.02 ± 0.05	I^-/I_3^-	$CoTe_2$@N-doped CNT	51
ZIF-67	16.27 ± 0.10	0.77 ± 0.03	59 ± 2	7.38 ± 0.08	I^-/I_3^-	Co_3O_4-WC-N-doped rGO	52
ZIF-67	16.21 ± 0.04	0.782 ± 0.008	62 ± 1	7.86 ± 0.05	I^-/I_3^-	$MoS_2@Co_3S_4$	53
ZIF-67	21.44	0.73	68	10.6	I^-/I_3^-	Co@Porous carbon	54
ZIF-67	18.4 ± 0.4	0.789 ± 0.005	64 ± 4	9.30 ± 0.17	I^-/I_3^-	$CoMoS_x$@Ni-$CoMoS_x$	55
ZIF-67	16.9	0.73	66	8.2	I^-/I_3^-	CoS_2@carbon nanocages	56
ZIF-7	16.40 ± 0.45	0.77	69 ± 1	8.69 ± 0.13	I^-/I_3^-	ZnSe/N-doped carbon	57
ZIF-8	13.58	0.836	71.49	8.12	$[Co(bpy)_3]^{2+/3+}$	ZnO–N-doped carbon	58
ZIF-8	18.88 ± 0.03	0.76 ± 0.01	69.79 ± 0.54	10.01 ± 0.04	I^-/I_3^-	SiO_2@N-doped carbon	59
ZIF-8	15.25 ± 0.09	0.77 ± 0.02	69.86 ± 1.03	8.20±.09	I^-/I_3^-	N-doped carbon sheet	60
ZIF-8	17.20	0.711	67	8.20	I^-/I_3^-	ZnS	61
Ni–Co–MOF	17.80 ± 0.09	0.780 ± 0.002	67 ± 1	9.30 ± 0.06	I^-/I_3^-	$NiCo_{0.2}$@C	62
Cu–TCPP	13.12 ± 0.10	0.89 ± 0.01	65.44 ± 1.01	7.61 ± 0.11	$[Co(bpy)_3]^{2+/3+}$	Cu_{2-x}Se@N-doped carbon	63
$Co_3[Co(CN)_6]_2$	16.8 ± 0.1	0.73 ± 0.01	70 ± 1	8.48 ± 0.04	I^-/I_3^-	CoS_x	64

Other	J_{sc} (mA cm^{-2})	V_{oc} (V)	FF (%)	PCE (%)	Function	Anode/Cathode	Ref.
MOF-5	7.95 ± 0.17	0.646 ± 0.006	68 ± 1	3.49 ± 0.04	Light scattering	ZnO/Pt	43
MOF-525	16.14 ± 0.13	0.8	70	8.91 ± 0.02	Cathode modifier	TiO_2/CC	65
UiO-66	18.6	0.678	60.8	7.67	Anode modifier	TiO_2/Graphene	6

Table 1 *(Contd.)*

Other	J_{sc} (mA cm^{-2})	V_{oc} (V)	FF (%)	PCE (%)	Function	Anode/Cathode	Ref.
MIL-125	10.9	0.85	69	6.4	Anode modifier	TiO_2/C	66
Ni-MOF	27.32	0.624	51.6	8.846	Anode modifier	TiO_2/Pt	67
Cu-btc	20.2	0.681	61.5	8.46	Anode modifier	TiO_2/Pt	68
Al-btc	16.67	0.756	69	8.69	Electrolyte	TiO_2/Pt	69
Mg-btc	12.6	0.69	55	4.80	Electrolyte	TiO_2/Pt	70
$[InK(ox)_2(H_2O)_4]_n$	16.54	0.73	62	7.42	Cosensitizer	TiO_2/Pt	7
$[In_{0.5}K(3\text{-qlc})_2Cl_{1.5}(H_2O)_{0.5}]_{2n}$	17.79	0.74	61	8.07	Cosensitizer	TiO_2/Pt	7
ZIF-8	10.28	0.753	69	5.34	Sorbent	TiO_2/Pt	5
ZIF-8	11.88	0.766	73.4	6.68	Sorbent	TiO_2/Pt	71

[a] Definition of abbreviations is given in the abbreviation list.

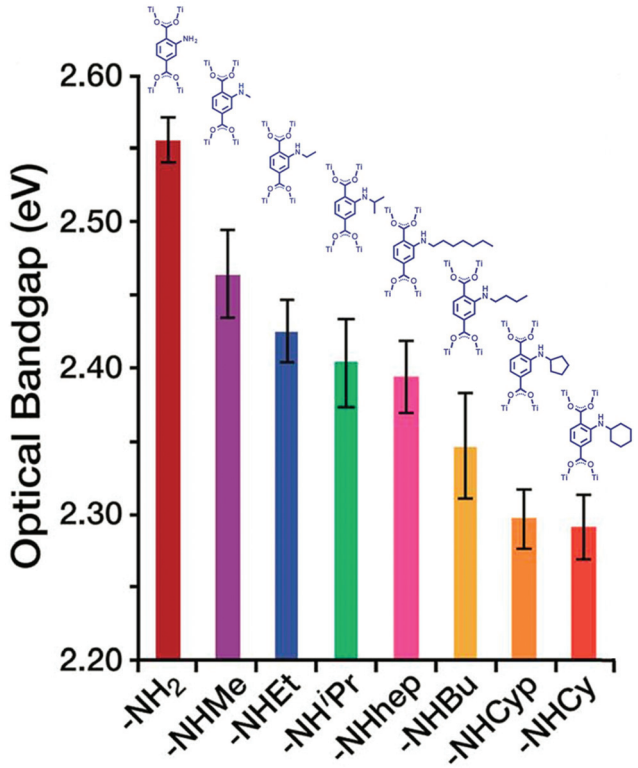

Fig. 2 Modification of bandgap in MIL-125-NHR by increasing side chain length. Adapted from ref. 80 with permission from the Royal Society of Chemistry.

To integrate MOFs in devices such as solar cells, it is necessary to fabricate surface-supportive MOF films.[89–91] The method of deposition itself has an immense effect on the cell performances. Charge transfer and guest loading are among the factors that are greatly influenced in films with defects, grain boundaries, or misoriented crystals.[92–94] All the methods utilized so far have their own advantages and drawbacks. For example, the solvothermal route, which is the most straightforward method for MOF thin film growth, produces films with rough surfaces and poor coverage mainly due to the lack of good control over nucleation. This problem is avoided in the stepwise (also known as layer-by-layer) deposition method. This method also offers a good control over crystal orientation and film thickness. However, in solution-based methods, the reactants must diffuse to the growth surface *via* a time-consuming process. In this regard, the vapor-based methods have shown promising results;[95] yet, the epitaxially grown MOF films (SURMOFs) are among the most widely used ones for cell fabrication.[96–100] In practical applications, MOF films are deposited on the surface of a metal oxide semiconductor film or directly on the surface of a conducting glass (ITO/FTO).[101] As demonstrated by Stavila *et al.*, Parsons *et al.*, and others, the quality of a MOF film is dependent on the properties of the substrate (roughness, porosity, surface functionality, *etc.*).[102–105]

While much attention has been paid to achieve efficient charge transport in MOFs,[106–111] studies on band alignment with other electronic materials are rather scarce. From a practical point of view, suitable alignment of the MOF LUMO and HOMO levels with the CB of TiO_2 and the redox potential of the electrolyte is critical for efficient photocurrent generation. Walsh *et al.* performed DFT calculations to theoretically determine the binding values of electrons in six porous frameworks. It was shown that in most cases (except for MIL-125), establishing an effective TiO_2/MOF electronic communication is poor.[112] Recently, laser spectroscopy studies have shown that the injection time constant of electrons at the TiO_2–MOF interface in a system consisting of iodine-doped $Cu_3(btc)_2$ is around 850 ps. The injection efficiency for this film, which was deposited on the surface of TiO_2 nanotubes *via* a solution-based stepwise method, was as low as 10%. However, when copper was replaced with ruthenium, the injection efficiency reached a maximum of 85%.[113] This is apparently due to the higher differences in the energy levels between the LUMO of $Ru_3(btc)_2$ and CB of TiO_2.[26,27] In addition to these, the thickness, morphology, and orientation of the crystals in a MOF film play dominant roles in the overall device performance.[24,29,114] For example, it has been shown that an effective electron injection can be established only by the very first MOF layers at interfacial contact with the underlying substrate (*e.g.,* TiO_2).[114,115] For chromophores located away but still within the energy hopping distance from the MOF–TiO_2 interface, electron injection can occur *via* RET models between neighboring sites (Fig. 3).[13,116] This highlights the importance of the structural features as well as the preparation methods, which ultimately govern the charge-transfer rates.[117]

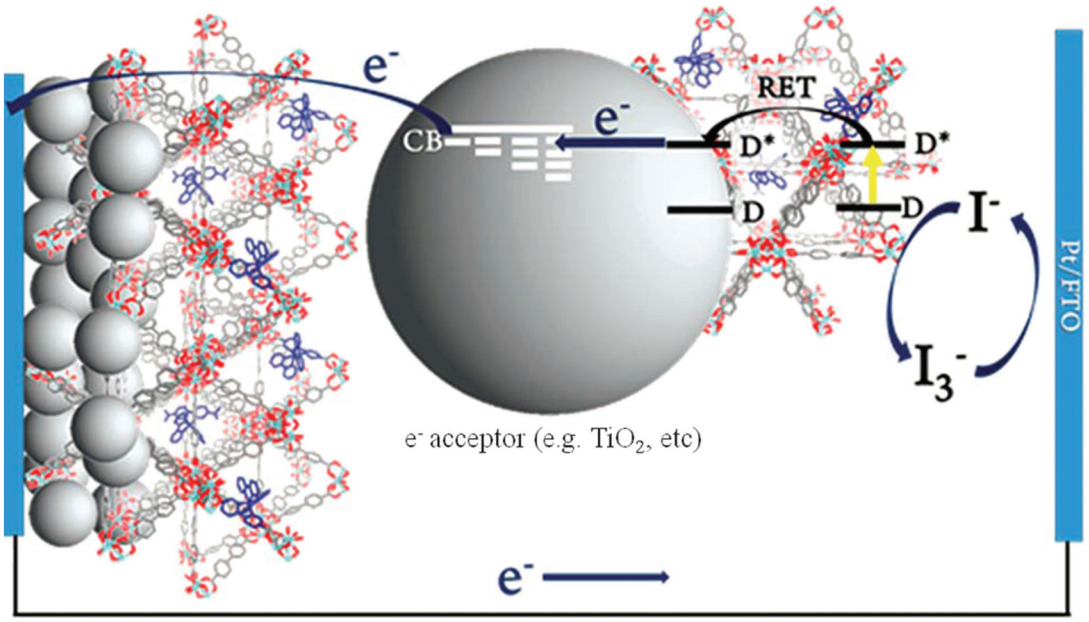

Fig. 3 Processes contributing to resonance energy transfer (RET) between chromophoric centres and charge separation at MOF-TiO_2 interfaces in a MOF-sensitized solar cell. Adapted from ref. 13 with permission from the Royal Society of Chemistry.

Crystal orientation can also affect charge transport. Recently, Hupp *et al.* reported an anisotropic behavior in the conductivity of NU-1000 thin films. In this case, the conductivity occurred through linker-to-linker electronic couplings between pairs of 1,3,6,8-tetrakis(*p*-benzoate)pyrenes located in the *a*,*b* plane of rod-shaped microcrystallites, when oriented almost perpendicular to the substrate surface. Under these conditions, redox hopping occurred along the *c* direction (Fig. 4). The authors attributed the boost in the conductivity to the reduced symmetry of NU-1000s' net topology (*csq*).[118] By applying a similar strategy, a 4.65 mA cm^{-2} current density was achieved for a [100]-oriented PPF-11 film grown on a ZnO substrate that is among the highest short circuit photocurrents (J_{sc}) reported for a MOF-sensitized solar cell, so far. The origin of such a high short-circuit current was attributed to the more facile in-plane charge movement through vertically aligned ZnTCPP chromophores.[29]

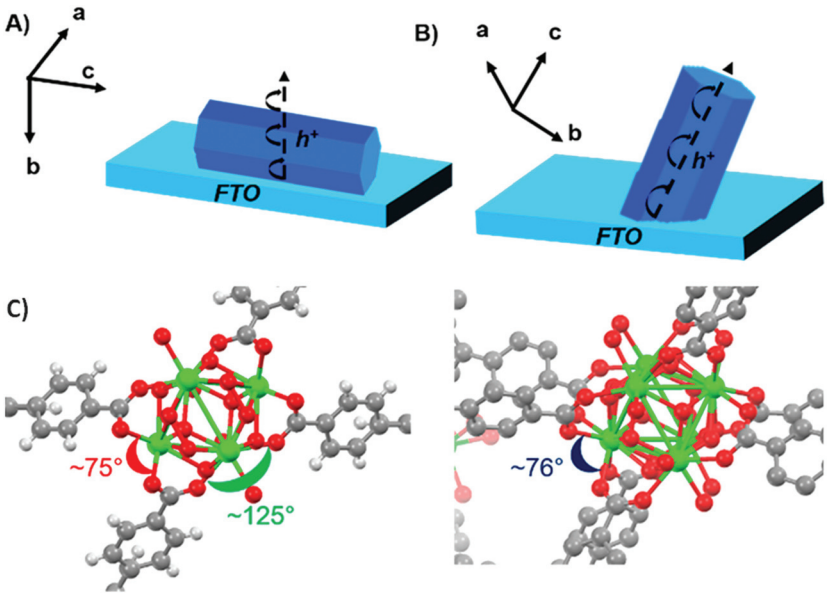

Fig. 4 Charge transport through microcrystallites of NU-1000, oriented with a hexagonal face in contact with electrode (A) or end-on oriented (B); illustration of the differences in siting the geometry for the various pairs of electronically coupled linkers based on O–Zr–O angles (C). Adapted with permission from ref. 118 copyright (2019) American Chemical Society.

Modification of the semiconductor surface/composition can contribute to superior cell performances as well.[25,33,66–68,71] For example, it has been reported that TiO_2 surface modification with DHBA reduces surface roughness, induces oriented growth, and inhibits charge recombination.[25,119] In addition to sensitization, it has been reported that MOFs can act as both sensitizers and hole transporting materials (HTMs), simultaneously. By coordination between Co^{II} and DAPV as a ligand, an output power conversion efficiency of 2.1% was achieved, which is remarkable for a MOF-sensitized solid state solar cell.[31]

Guest@MOF

The guest@MOF approach utilizes the inherent porosity of MOFs and host–guest interactions to induce conductivity by loading electroactive guest molecules into the framework. In this approach, the use of MOFs as sorbents can be explained in two ways. In one approach, no significant interactions between the guest molecules and the framework were observed. In other words, in this approach, molecules such as classical dyes are just physically encapsulated by the MOF. A prime example is the work of Li *et al.*, who utilized a 2 nm thick ZIF-8 film as a scaffold for the uptake of a number of dyes such as N719.[5,71] The authors concluded that the introduction of ZIF-8 on TiO_2 film creates a barrier against charge recombination and improves the V_{oc} of the cell.[5] The other approach (also known as the guest-promoted approach) involves a relatively strong bonding between the guest and the MOF and ultimately provides the donor–acceptor pathways for charge transport. These interactions range from covalent bonding to weaker forces such as π–π stacking interactions.[120,121] A survey of the literature shows that guest molecules that have been recently employed for the construction of electroactive MOFs are 7,7,8,8-tetra-cyanoquinodimethane (TCNQ), C_{60} fullerene, ferrocene, iodine, TTF, and recently, cadmium.[32,122–132] The *ab initio* calculations demonstrated that binding TCNQ to two neighboring Cu sites in the SBUs of $Cu_3(btc)_2$ inserts unoccupied molecular orbitals into the MOF HOMO–LUMO gap and increases the conductivity *via* a system which is best described by a through-bond model (Fig. 5).[123] However, the node cross-linking strategy is feasible only when unsaturated metal sites are available. A challenge in achieving higher conductivity in guest-loaded frameworks is the trade-off between pore size and electron/ion diffusion rates. Although it is generally accepted that pore diameter should be smaller than exciton diffusion distance,[133] Morris's group has recently demonstrated that the overall charge-transfer rate in a number of ferrocene-doped MOF thin films is mainly dependent on the ion diffusion rate (rather than electron) and increases with an increase in the pore size.[117] This work highlighted the importance of ion–MOF interaction in determining the charge transfer rate.

Heinke *et al.* developed a C_{60}-loaded Zn-porphyrin SURMOF through a stepwise spin coating process, in which the photosensitive porphyrins acted as the electron donors and the C_{60} molecules as the electron acceptors. In this case, a 2-order of magnitude improvement was observed in the conductivity of the C_{60}-containing framework ($\sim 10^{-11}$ S cm^{-1}) due to the efficient charge separation.[127] As another promising approach, a recent study showed that structural modifications at the *meso* position can influence the degree of host–guest interactions between porphyrin-based donors and C_{60}-based acceptors.[131] Similarly, Morsali *et al.* succeeded in increasing the conductivity of an amine-containing MOF (TMU-60) from 5.3×10^{-5} to 1.8×10^{-2} S cm^{-1} *via* the sorption of electroactive Cd^{II} ions.[129] Supramolecular interactions between cadmium ions and the free electrons of nitrogen atoms of the ligand and the electrostatic interactions between the cations and the dipoles of nitrogen atoms of the ligand resulted in electron hopping between the metal nodes and localized Cd ions. Interestingly, the authors observed no significant increase in the conductivity of UiO-66, MIL-100(Fe), and HKUST-1 under similar conditions.[129] Allendorf *et al.* demonstrated the exciting possibility of tuning the guest@MOF strategy by the simultaneous confinement of donor and acceptor pairs in MOF-177.[133] This study is an interesting example in which all components functioned as active parts in the energy conversion process. In this system, the framework material served as

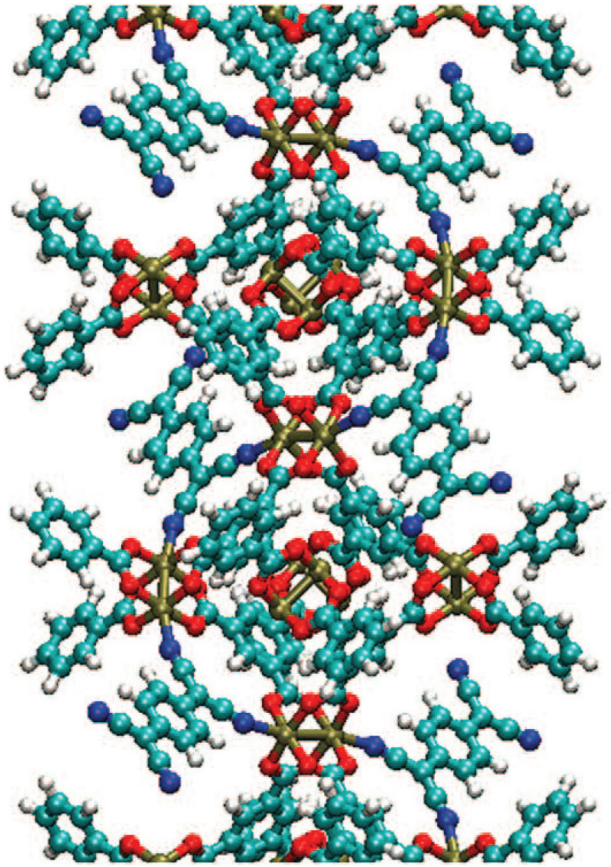

Fig. 5 Structure of TCNQ@$Cu_3(btc)_2$ with a covalent charge-transport pathway *via* Cu-TCNQ linkages. Adapted with permission from ref. 123 copyright (2014) American Association for the Advancement of Science.

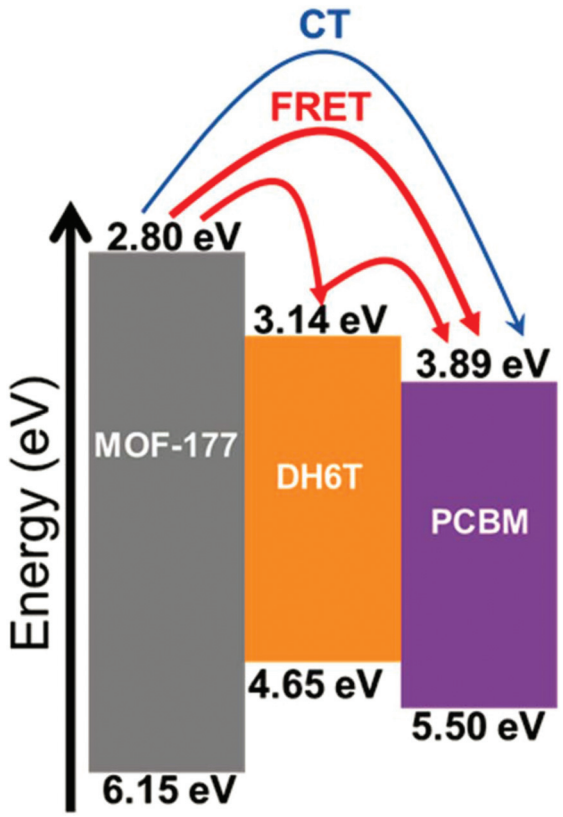

Fig. 6 Band alignment and energy/charge transfer between MOF-177 (scaffold), DH6T (donor), and PCBM (acceptor). Definition of abbreviations is given in the abbreviation list. Reproduced from ref. 133 with permission from the Royal Society of Chemistry.

an antenna and caused FRET to occur between the btc linkers and DH6T molecules (Fig. 6).

It is worth mentioning that the compatibility of the redox electrolyte and guest molecules has a crucial effect on the performance of the cell. For guest-loaded MOFs, charge transport can be affected by the choice of redox shuttle used in the cell. For example, while it has been shown that the inclusion of iodine molecules (in acetonitrile) in liquid cells (that consist of I^-/I_3^- in the mixture of acetonitrile and valeronitrile) is beneficial for the cell performance,[26,27,32,33] C_{60}-loaded PPF-11 displayed no measurable conductivity and much weaker photovoltaic response in the presence of the same electrolyte.[29]

MOF-derived electrodes

Over past years, MOFs have proven to be suitable templates/precursors for the fabrication of carbon-/metal-based porous materials and thus MOF-derived materials are being used both in photoanodes and cathodes. The inherent properties of the parent MOF (such as ordered porous structure and high surface area) can be utilized to prepare functional materials with new properties. The morphology, porosity, and size of the obtained structures are highly dependent on the preparation conditions like heating temperature, time, rate, and atmosphere (air or inert gas).

To date, MOF-derived electrodes have been prepared by pyrolysis or calcination of MOFs such as MIL-125(Ti),[37,38,40,41] MOF-5,[43,134] ZIF-7,[57] ZIF-8,[58–61] and ZIF-67.[50,52–54,56] Some essential characteristics of metal oxides (TiO_2, ZnO) in photoanodes, such as light absorption and scattering and charge transport, can be tuned through precisely controlling the particle and pore size of MOF-derived structures.[40,42] This could be achieved by the addition of structure-directing agents.[39,41] For example, Park *et al.* used an amphiphilic graft copolymer of poly(vinylchloride)-graft-poly(oxyethylene methacrylate) to prepare mesoporous TiO_2 structures from MIL-125(Ti). With a TiO_2 film thickness of 10 μm, a 34% improvement in the amount of adsorbed dyes was obtained (surface area 98.3 m^2 g^{-1}), and when this film was used in solid state/liquid junction solar cells, power conversion efficiencies of 7.45 and 8.43% were reached, while standard films (made from commercial metal oxide) with the same thickness gave 5.36 and 7.14% under the same test conditions.[41] Some authors also reported a templating role for counter ions in enabling the aggregation of smaller fragments to form diverse morphologies.[44] In addition, controlling the heating conditions (rate/time) during thermal treatment is another key factor for maintaining the initial morphology of the parent MOF.[42]

An ideal cathode material should be able to provide conductivity, stability, and electrocatalytic reduction of the electrolyte (*e.g.*, triiodide). To date, Pt, transition metal sulfides, as well as carbon-based materials (*e.g.* carbon black, graphene, and SWCNT) have been used as cathode materials in DSSCs. Recently, Wang *et al.* developed a cathode material comprising CoX_2–N-doped carbon hybrids (X = S, Se) derived from the pyrolysis of ZIF-67 polyhedra by the doctor blade method (Fig. 7).[49] In this hybrid, the role of nitrogen-doped carbon was electronic conduction while the CoX_2 species provided abundant catalytic centres. While the specific morphology of the materials contributed to fast electrolyte access, cathodes with softer atoms (selenium) achieved a higher photon to current conversion efficiency (~9%). The deposition of MOF-derived material can be carried out using *in situ* methods. Recently, a cobalt-metalloporphyrin MOF thin film was prepared on an FTO substrate *via* the LPE approach. When a $CoS_{1.097}$@N-doped carbon cathode was fabricated into the DSSC, a 9.11% efficiency was achieved.[45] Doping heteroatoms to improve the electrocatalytic activity has been demonstrated by incorporating bimetallic/metalloid additives in the structure of the cathode material.[48,51,62,135] A charge transfer resistance (R_{ct}) as low as 0.192 Ω was achieved for a ZIF-67-derived cathode that was comprised of hollow polyhedrons of $CoMoS_x$@Ni-$CoMoS_x$ and the device showed 89% reduction in R_{ct} in comparison with a platinized reference.[55] Particle size influences R_{ct} as well. It has been shown that in cathodes with smaller CoS particles, the value of the roughness factor is higher. This provides more catalytic sites for triiodide ions in the electrolyte, thus improving FF and power conversion efficiency.[46]

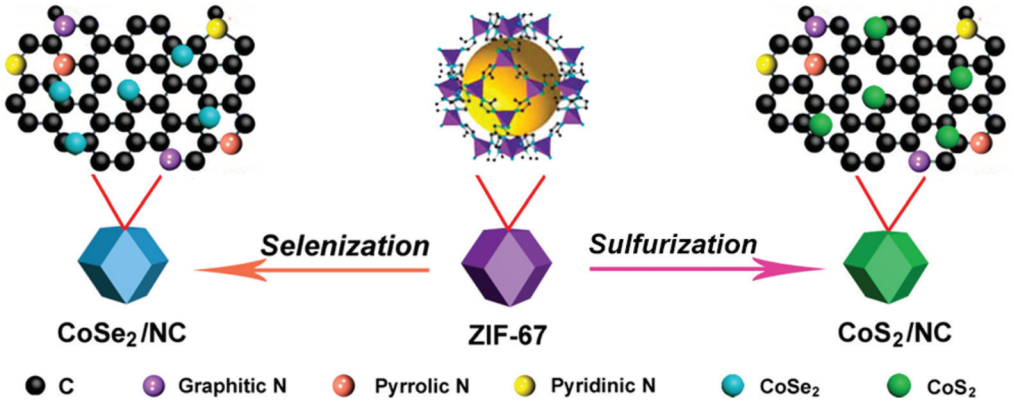

Fig. 7 Illustration of the synthesis and structure of $CoSe_2$/NC and CoS_2/NC hybrids. Reproduced with permission from ref. 49 copyright 2019 American Chemical Society.

Conclusions and perspectives

The prospect of integrating MOFs in devices such as solar cells has led researchers to the point where significant progress has been made today. Nonetheless, there is still some way to go in order to achieve high efficiencies. Tuning MOF composition and structure are expected to improve DSSC device performances. For MOF-sensitized solar cells, as discussed, the first step begins with the development of appropriately designed MOFs with improved solar light harvesting and exciton-transport features. In this regard, the use of natural mimicking structures like porphyrinic MOFs has shown promising results. On the one hand, by employing photosensitization methods such as co-sensitization with QDs or by the introduction of appropriate functional groups, the photon capture characteristics of porphyrin arrays could be improved. On the other hand, the incorporation of suitable guest molecules can increase the host–guest interactions and promote exciton diffusion. A detailed understanding of the structure–property correlation in view of exciton migration would be of great interest. From a preparative perspective, the development of deposition methods in which the distance and orientation between chromophoric sites are precisely controlled also facilitates exciton migration. Indeed, in this scope, thin layers of homogeneous SURMOFs with highly oriented crystals have advantages over powder forms of MOFs or polycrystalline MOF films and can provide conditions under which most photoactive moieties within the MOF film can be excited. However, the stability and adhesion of the film to the support (*e.g.* TiO_2 and TCO) as well as the interface phenomena (*e.g.* band alignment and charge injection) should also be taken into account. Proper positions of the energy levels at the MOF oxide/electrolyte interfaces are important for efficient photocurrent generation.

Long-range ordering, high surface area, porosity, and specific pore size of MOFs have made MOF-derived materials ideal electrode materials. However, developments of new strategies in which synthetic conditions are carefully controlled are essential for obtaining materials with desired morphology, size, and composition for efficient electrochemical processes. In addition, understanding the electrochemical processes of MOF-derived materials still needs further studies in order to gain insights into the correlation between the structural changes during catalyst preparation and the electrochemical activities.

List of abbreviations

BDC	1,4-Benzenedicarboxylate
BPY	2,2′-Bipyridyl/4,4′-Bipyridyl
BTC	1,3,5-Benzenetricarboxylate
CB	Conduction band
CC	Carbon cloth
CN	Cyanide
CNT	Carbon nanotube
CT	Charge transfer
DAPV	Di(3-diaminopropyl)-viologen
DCBPY	5,5′-Dicarboxy-2,2′-bipyridine
DFT	Density functional theory
DHBA	3,4-Dihydroxybenzoic acid
DH6T	α,ω-Dihexylsexithiophene
DMB	1,4-Dimethoxybenzene
DPA	Diphenylamine
DSSC	Dye-sensitized solar cell
FF	Fill factor
FRET	Förster resonance energy transfer
FTO	Fluorine-doped tin oxide
HER	Hydrogen evolution reaction
HKUST	Hong Kong University of Science and Technology
HOMO	Highest occupied molecular orbital
H_4TBAPy	4,4′,4″,4‴-(Pyrene-1,3,6,8-tetrayl)tetrabenzoic acid
HTM	Hole transporting material
ITO	Indium tin oxide

J_{sc}	Short-circuit current density
LPE	Liquid-phase epitaxy
LUMO	Lowest unoccupied molecular orbital
MIL	Material of Institut Lavoisier
MOF	Metal–organic framework
MOFSC/MSSC	Metal–organic framework-sensitized solar cell
MWCNT	Multi-walled carbon nanotube
NDC	2,6-Naphthalenedicarboxylate
NT	Nanotube
NTU	Nanyang Technological University
NU	Northwestern University
OX	Oxalate
PCBM	[6,6]-Phenyl-C_{61}-butyric acid methyl ester
PIZA-1	Porphyrinic illinois zeolite analogue no. 1
PPF	Porphyrin paddlewheel framework
QD	Quantum dot
QLC	Quinoline-3-carboxylate
R_{ct}	Charge transfer resistance
RET	Resonance energy transfer
rGO	Reduced graphene oxide
SBU	Secondary building units
SURMOF	Surface-mounted metal–organic framework
SWCNT	Single-walled carbon nanotube
TCNQ	7,7,8,8-Tetra-cyanoquinodimethane
TCO	Transparent conductive oxide
TCPP	Tetrakis(4-carboxyphenyl)porphyrin
TMU	Tarbiat Modares University
TTF	Tetrathiafulvalene
UiO	Universitetet i Oslo
V_{oc}	Open circuit voltage
WC	Tungsten carbide
ZIF	Zeolitic imidazolate framework

Conflicts of interest

There are no conflicts to declare.

Acknowledgements

M. M. gratefully acknowledges the financial support from the Ferdowsi University of Mashhad (Grant No. 73209), the Iran Science Elites Federation (ISEF), Zeolite and Porous Materials Committee of Iranian Chemical Society and the Iran National Science Foundation (INSF). M. M. also acknowledges the Cambridge Crystallographic Data Centre (CCDC) for access to the Cambridge Structural Database.

Notes and references

1 A. Hagfeldt, G. Boschloo, L. Sun, L. Kloo and H. Pettersson, *Chem. Rev.*, 2010, **110**, 6595–6663.
2 M. Alvaro, E. Carbonell, B. Ferrer, F. X. Llabrés i Xamena and H. Garcia, *Chem. – Eur. J.*, 2007, **13**, 5106–5112.
3 F. X. Llabrés i Xamena, A. Corma and H. Garcia, *J. Phys. Chem. C*, 2007, **111**, 80–85.
4 P. L. Feng, J. J. Perry IV, S. Nikodemski, B. W. Jacobs, S. T. Meek and M. D. Allendorf, *J. Am. Chem. Soc.*, 2010, **132**, 15487–15489.
5 Y. Li, A. Pang, C. Wang and M. Wei, *J. Mater. Chem.*, 2011, **21**, 17259–17264.
6 Y. He, Z. Zhang, W. Wang and L. Fu, *J. Alloys Compd.*, 2020, **825**, 154089.
7 X. Du, R. Fan, X. Wang, G. Yu, L. Qiang, P. Wang, S. Gao and Y. Yang, *Cryst. Growth Des.*, 2016, **16**, 1737–1745.
8 B. Tahmouresilerd, P. J. Larson, D. K. Unruh and A. F. Cozzolino, *Catal. Sci. Technol.*, 2018, **8**, 4349–4357.
9 M. Samaniyan, M. Mirzaei, R. Khajavian, H. Eshtiagh-Hosseini and C. Streb, *ACS Catal.*, 2019, **9**, 10174–10191.
10 B. M. Connolly, D. G. Madden, A. E. Wheatley and D. Fairen-Jimenez, *J. Am. Chem. Soc.*, 2020, **142**, 8541–8549.
11 F. Carraro, M. d. J. Velásquez-Hernández, E. Astria, W. Liang, L. Twight, C. Parise, M. Ge, Z. Huang, R. Ricco, X. Zou, L. Villanova, C. O. Kappe, C. Doonan and P. Falcaro, *Chem. Sci.*, 2020, **11**, 3397–3404.
12 H. Furukawa, K. E. Cordova, M. O'Keeffe and O. M. Yaghi, *Science*, 2013, **341**, 1230444.
13 W. A. Maza, A. J. Haring, S. R. Ahrenholtz, C. C. Epley, S. Lin and A. J. Morris, *Chem. Sci.*, 2016, **7**, 719–727.
14 E. D. Spoerke, L. J. Small, M. E. Foster, J. Wheeler, A. M. Ullman, V. Stavila, M. Rodriguez and M. D. Allendorf, *J. Phys. Chem. C*, 2017, **121**, 4816–4824.
15 M. D. Allendorf, A. Schwartzberg, V. Stavila and A. A. Talin, *Chem. – Eur. J.*, 2011, **17**, 11372–11388.
16 R. Kaur, K.-H. Kim, A. Paul and A. Deep, *J. Mater. Chem. A*, 2016, **4**, 3991–4002.
17 C.-C. Chueh, C.-I. Chen, Y.-A. Su, H. Konnerth, Y.-J. Gu, C.-W. Kung and K. C.-W. Wu, *J. Mater. Chem. A*, 2019, **7**, 17079–17095.
18 S. Kuyuldar, D. T. Genna and C. Burda, *J. Mater. Chem. A*, 2019, **7**, 21545–21576.
19 C. H. Hendon, D. Tiana and A. Walsh, *Phys. Chem. Chem. Phys.*, 2012, **14**, 13120–13132.
20 V. Stavila, A. A. Talin and M. D. Allendorf, *Chem. Soc. Rev.*, 2014, **43**, 5994–6010.
21 I. Stassen, N. Burtch, A. Talin, P. Falcaro, M. Allendorf and R. Ameloot, *Chem. Soc. Rev.*, 2017, **46**, 3185–3241.
22 M. D. Allendorf, R. Dong, X. Feng, S. Kaskel, D. Matoga and V. Stavila, *Chem. Rev.*, 2020, **120**, 8581–8640.
23 A. Santiago Portillo, H. G. Baldoví, M. T. Garcia Fernandez, S. Navalon, P. Atienzar, B. Ferrer, M. Alvaro, H. Garcia and Z. Li, *J. Phys. Chem. C*, 2017, **121**, 7015–7024.
24 R. Khajavian and K. Ghani, *J. Solid State Chem.*, 2018, **262**, 94–99.
25 R. Khajavian and K. Ghani, *J. Cryst. Growth*, 2016, **455**, 60–65.

26 D. Y. Lee, D. V. Shinde, S. J. Yoon, K. N. Cho, W. Lee, N. K. Shrestha and S.-H. Han, *J. Phys. Chem. C*, 2014, **118**, 16328–16334.
27 D. Y. Lee, E.-K. Kim, C. Y. Shin, D. V. Shinde, W. Lee, N. K. Shrestha, J. K. Lee and S.-H. Han, *RSC Adv.*, 2014, **4**, 12037–12042.
28 H. A. Lopez, A. Dhakshinamoorthy, B. Ferrer, P. Atienzar, M. Alvaro and H. Garcia, *J. Phys. Chem. C*, 2011, **115**, 22200–22206.
29 M. A. Gordillo, D. K. Panda and S. Saha, *ACS Appl. Mater. Interfaces*, 2019, **11**, 3196–3206.
30 R. Kaur, K.-H. Kim and A. Deep, *Appl. Surf. Sci.*, 2017, **396**, 1303–1309.
31 D. Y. Ahn, D. Y. Lee, C. Y. Shin, H. T. Bui, N. K. Shrestha, L. Giebeler, Y.-Y. Noh and S.-H. Han, *ACS Appl. Mater. Interfaces*, 2017, **9**, 12930–12935.
32 D. Y. Lee, I. Lim, C. Y. Shin, S. A. Patil, W. Lee, N. K. Shrestha, J. K. Lee and S.-H. Han, *J. Mater. Chem. A*, 2015, **3**, 22669–22676.
33 D. Y. Lee, C. Y. Shin, S. J. Yoon, H. Y. Lee, W. Lee, N. K. Shrestha, J. K. Lee and S.-H. Han, *Sci. Rep.*, 2015, **4**, 3930.
34 T. H. Chang, C. W. Kung, H. W. Chen, T. Y. Huang, S. Y. Kao, H. C. Lu, M. H. Lee, K. M. Boopathi, C. W. Chu and K. C. Ho, *Adv. Mater.*, 2015, **27**, 7229–7235.
35 R. Kaur, A. L. Sharma, K.-H. Kim and A. Deep, *J. Ind. Eng. Chem.*, 2017, **53**, 77–81.
36 R. Kaur, A. Rana, R. K. Singh, V. A. Chhabra, K.-H. Kim and A. Deep, *RSC Adv.*, 2017, **7**, 29015–29024.
37 J. Dou, Y. Li, F. Xie, X. Ding and M. Wei, *Cryst. Growth Des.*, 2016, **16**, 121–125.
38 R. Tang, Z. Xie, S. Zhou, Y. Zhang, Z. Yuan, L. Zhang and L. Yin, *ACS Appl. Mater. Interfaces*, 2016, **8**, 22201–22212.
39 W. S. Chi, D. K. Roh, C. S. Lee and J. H. Kim, *J. Mater. Chem. A*, 2015, **3**, 21599–21608.
40 R. Tang, R. Yin, S. Zhou, T. Ge, Z. Yuan, L. Zhang and L. Yin, *J. Mater. Chem. A*, 2017, **5**, 4962–4971.
41 J. T. Park, J. Moon, G. H. Choi, S. M. Lim and J. H. Kim, *J. Ind. Eng. Chem.*, 2020, **84**, 384–392.
42 T. Enomoto, S. Ueno, E. Hosono, M. Hagiwara and S. Fujihara, *CrystEngComm*, 2017, **19**, 2844–2851.
43 Y. Li, Z. Che, X. Sun, J. Dou and M. Wei, *Chem. Commun.*, 2014, **50**, 9769–9772.
44 T. Kundu, S. C. Sahoo and R. Banerjee, *Cryst. Growth Des.*, 2012, **12**, 2572–2578.
45 J. Ou, J. Xiang, J. Liu and L. Sun, *ACS Appl. Mater. Interfaces*, 2019, **11**, 14862–14870.
46 S.-H. Hsu, C.-T. Li, H.-T. Chien, R. R. Salunkhe, N. Suzuki, Y. Yamauchi, K.-C. Ho and K. C.-W. Wu, *Sci. Rep.*, 2015, **4**, 6983.
47 J. Ou, C. Gong, J. Xiang and J. Liu, *Sol. Energy*, 2018, **174**, 225–230.
48 Z. Xie, X. Cui, W. Xu and Y. Wang, *Electrochim. Acta*, 2017, **229**, 361–370.
49 X. Wang, Y. Xie, B. Bateer, K. Pan, X. Zhang, J. Wu and H. Fu, *ACS Sustainable Chem. Eng.*, 2019, **7**, 2784–2791.
50 Y. Li, X. Liu, H. Li, D. Shi, Q. Jiao, Y. Zhao, C. Feng, X. Bai, H. Wang and Q. Wu, *J. Power Sources*, 2019, **422**, 122–130.
51 S. Huang, S. Li, Q. He, H. An, L. Xiao and L. Hou, *Appl. Surf. Sci.*, 2019, **476**, 769–777.
52 L. Chen, W. Chen and E. Wang, *J. Power Sources*, 2018, **380**, 18–25.
53 S. a. Liu, Z. Li, K. Zhao, M. Hao, Z. Zhang, L. Li, Y. Zhang and W. Zhang, *J. Alloys Compd.*, 2020, **831**, 154910.
54 M.-S. Wu, Y.-C. Hou and J.-C. Lin, *J. Alloys Compd.*, 2019, **778**, 662–668.
55 X. Qian, W. Wu, J. Zhuang, Y. Niu, J. Huang and L. Hou, *J. Power Sources*, 2019, **417**, 21–28.
56 X. Cui, Z. Xie and Y. Wang, *Nanoscale*, 2016, **8**, 11984–11992.
57 S.-L. Jian, Y.-J. Huang, M.-H. Yeh and K.-C. Ho, *J. Mater. Chem. A*, 2018, **6**, 5107–5118.
58 A. S. Ahmed, W. Xiang, I. S. Amiinu, Z. Li, R. Yu and X. Zhao, *Sustainable Energy Fuels*, 2019, **3**, 1976–1987.
59 A. S. Ahmed, W. Xiang, Z. Li, I. S. Amiinu and X. Zhao, *Electrochim. Acta*, 2018, **292**, 276–284.
60 J. Ou, C. Gong, M. Wang, J. Xiang and J. Liu, *Electrochim. Acta*, 2018, **286**, 212–218.
61 Y. Zhao, B. Song, X. Cui, Y. Ren, W. Yue and Y. Wang, *Mater. Lett.*, 2019, **250**, 193–196.
62 X. Jiang, H. Li, S. Li, S. Huang, C. Zhu and L. Hou, *Chem. Eng. J.*, 2018, **334**, 419–431.
63 J. Ou, B. Hu, S. He, W. Wang and Y. Han, *Sol. Energy*, 2020, **201**, 693–700.
64 M. S. Kim and J. H. Bang, *J. Phys. Chem. C*, 2018, **122**, 13267–13276.
65 T.-Y. Chen, Y.-J. Huang, C.-T. Li, C.-W. Kung, R. Vittal and K.-C. Ho, *Nano Energy*, 2017, **32**, 19–27.
66 A. V. Vinogradov, H. Zaake-Hertling, E. Hey-Hawkins, A. V. Agafonov, G. Seisenbaeva, V. Kessler and V. V. Vinogradov, *Chem. Commun.*, 2014, **50**, 10210–10213.
67 V. Ramasubbu, P. R. Kumar, E. M. Mothi, K. Karuppasamy, H.-S. Kim, T. Maiyalagan and X. S. Shajan, *Appl. Surf. Sci.*, 2019, **496**, 143646.
68 B. Tang, L. Ji, Y. Dai, H. Chen, Z. Zhang, Z. Wang and S. Li, *Nano*, 2020, **15**, 2050055.
69 J. Fan, L. Li, H.-S. Rao, Q.-L. Yang, J. Zhang, H.-Y. Chen, L. Chen, D.-B. Kuang and C.-Y. Su, *J. Mater. Chem. A*, 2014, **2**, 15406–15413.
70 F. Bella, R. Bongiovanni, R. S. Kumar, M. A. Kulandainathan and A. M. Stephan, *J. Mater. Chem. A*, 2013, **1**, 9033–9036.
71 Y. Li, C. Chen, X. Sun, J. Dou and M. Wei, *ChemSusChem*, 2014, **7**, 2469–2472.
72 C. Y. Lee, O. K. Farha, B. J. Hong, A. A. Sarjeant, S. T. Nguyen and J. T. Hupp, *J. Am. Chem. Soc.*, 2011, **133**, 15858–15861.
73 H.-J. Son, S. Jin, S. Patwardhan, S. J. Wezenberg, N. C. Jeong, M. So, C. E. Wilmer, A. A. Sarjeant, G. C. Schatz, R. Q. Snurr, O. K. Farha, G. P. Wiederrecht and J. T. Hupp, *J. Am. Chem. Soc.*, 2013, **135**, 862–869.

74 S. R. Ahrenholtz, C. C. Epley and A. J. Morris, *J. Am. Chem. Soc.*, 2014, **136**, 2464–2472.
75 K. M. Ishihara and F. Tian, *Langmuir*, 2018, **34**, 15689–15699.
76 J. Liu, W. Zhou, J. Liu, I. Howard, G. Kilibarda, S. Schlabach, D. Coupry, M. Addicoat, S. Yoneda and Y. Tsutsui, *Angew. Chem., Int. Ed.*, 2015, **54**, 7441–7445.
77 C.-K. Lin, D. Zhao, W.-Y. Gao, Z. Yang, J. Ye, T. Xu, Q. Ge, S. Ma and D.-J. Liu, *Inorg. Chem.*, 2012, **51**, 9039–9044.
78 M. A. Syzgantseva, N. F. Stepanov and O. A. Syzgantseva, *ACS Appl. Mater. Interfaces*, 2020, **12**, 17611–17619.
79 H. L. Nguyen, T. T. Vu, D. Le, T. L. Doan, V. Q. Nguyen and N. T. Phan, *ACS Catal.*, 2017, **7**, 338–342.
80 M. W. Logan, S. Ayad, J. D. Adamson, T. Dilbeck, K. Hanson and F. J. Uribe-Romo, *J. Mater. Chem. A*, 2017, **5**, 11854–11863.
81 J. Liu, W. Zhou, J. Liu, Y. Fujimori, T. Higashino, H. Imahori, X. Jiang, J. Zhao, T. Sakurai and Y. Hattori, *J. Mater. Chem. A*, 2016, **4**, 12739–12747.
82 A. S. Yasin, J. Li, N. Wu and T. Musho, *Phys. Chem. Chem. Phys.*, 2016, **18**, 12748–12754.
83 A. Cadiau, N. Kolobov, S. Srinivasan, M. G. Goesten, H. Haspel, A. V. Bavykina, M. R. Tchalala, P. Maity, A. Goryachev, A. S. Poryvaev, M. Eddaoudi, M. V. Fedin, O. F. Mohammed and J. Gascon, *Angew. Chem., Int. Ed.*, 2020, **132**, 13570–13574.
84 W. A. Maza and A. J. Morris, *J. Phys. Chem. C*, 2014, **118**, 8803–8817.
85 P. Karthik, A. M. Shaheer, A. Vinu and B. Neppolian, *Small*, 2020, **16**, 1902990.
86 S. Jin, H.-J. Son, O. K. Farha, G. P. Wiederrecht and J. T. Hupp, *J. Am. Chem. Soc.*, 2013, **135**, 955–958.
87 Z. Chen, Z.-G. Gu, W.-Q. Fu, F. Wang and J. Zhang, *ACS Appl. Mater. Interfaces*, 2016, **8**, 28737–28742.
88 W. Lv, L. Li, M. Xu, J. Hong, X. Tang, L. Xu, Y. Wu, R. Zhu, R. Chen and W. Huang, *Adv. Mater.*, 2019, **31**, 1900682.
89 V. Chernikova, O. Shekhah and M. Eddaoudi, *ACS Appl. Mater. Interfaces*, 2016, **8**, 20459–20464.
90 R. Khajavian and K. Ghani, *CrystEngComm*, 2018, **20**, 1546–1552.
91 A. L. Semrau, S. Wannapaiboon, S. P. Pujari, P. Vervoorts, B. Albada, H. Zuilhof and R. A. Fischer, *Cryst. Growth Des.*, 2019, **19**, 1738–1747.
92 L. Heinke, Z. Gu and C. Wöll, *Nat. Commun.*, 2014, **5**, 4562.
93 M. D. Allendorf and V. Stavila, *Nat. Mater.*, 2016, **15**, 255–257.
94 K. Müller, K. Fink, L. Schöttner, M. Koenig, L. Heinke and C. Wöll, *ACS Appl. Mater. Interfaces*, 2017, **9**, 37463–37467.
95 I. Stassen, M. Styles, G. Grenci, H. Van Gorp, W. Vanderlinden, S. De Feyter, P. Falcaro, D. De Vos, P. Vereecken and R. Ameloot, *Nat. Mater.*, 2016, **15**, 304–310.
96 H. Gliemann and C. Wöll, *Mater. Today*, 2012, **15**, 110–116.
97 J.-L. Zhuang, A. Terfort and C. Wöll, *Coord. Chem. Rev.*, 2016, **307**, 391–424.
98 J. Liu and C. Wöll, *Chem. Soc. Rev.*, 2017, **46**, 5730–5770.
99 Z.-G. Gu and J. Zhang, *Coord. Chem. Rev.*, 2019, **378**, 513–532.
100 Z. Wang and C. Wöll, *Adv. Mater. Technol.*, 2019, **4**, 1800413.
101 G. Genesio, J. Maynadié, M. Carboni and D. Meyer, *New J. Chem.*, 2018, **42**, 2351–2363.
102 V. Stavila, J. Volponi, A. M. Katzenmeyer, M. C. Dixon and M. D. Allendorf, *Chem. Sci.*, 2012, **3**, 1531–1540.
103 M. C. So, S. Jin, H.-J. Son, G. P. Wiederrecht, O. K. Farha and J. T. Hupp, *J. Am. Chem. Soc.*, 2013, **135**, 15698–15701.
104 D. T. Lee, J. Zhao, C. J. Oldham, G. W. Peterson and G. N. Parsons, *ACS Appl. Mater. Interfaces*, 2017, **9**, 44847–44855.
105 A. I. Zvyagina, A. A. Shiryaev, A. E. Baranchikov, V. V. Chernyshev, Y. Y. Enakieva, O. A. Raitman, A. A. Ezhov, I. N. Meshkov, D. A. Grishanov, O. S. Ivanova, Y. G. Gorbunova, V. V. Arslanova and M. A. Kalinina, *New J. Chem.*, 2017, **41**, 948–957.
106 A. Pathak, J.-W. Shen, M. Usman, L.-F. Wei, S. Mendiratta, Y.-S. Chang, B. Sainbileg, C.-M. Ngue, R.-S. Chen, M. Hayashi, T.-T. Luo, F.-R. Chen, K.-H. Chen, T.-W. Tseng, L.-C. Chen and K.-L. Lu, *Nat. Commun.*, 2019, **10**, 1721.
107 L. S. Xie, G. Skorupskii and M. Dincă, *Chem. Rev.*, 2020, **120**, 8536–8580.
108 C.-W. Kung, S. Goswami, I. Hod, T. C. Wang, J. Duan, O. K. Farha and J. T. Hupp, *Acc. Chem. Res.*, 2020, **53**, 1187–1195.
109 G. Skorupskii, B. A. Trump, T. W. Kasel, C. M. Brown, C. H. Hendon and M. Dincă, *Nat. Chem.*, 2020, **12**, 131–136.
110 M. J. Golomb, J. Calbo, J. K. Bristow and A. Walsh, *J. Mater. Chem. A*, 2020, **8**, 13160–13165.
111 L. S. Xie, S. S. Park, M. J. Chmielewski, H. Liu, R. A. Kharod, L. Yang, M. G. Campbell and M. Dincă, *Angew. Chem., Int. Ed.*, 2020, DOI: 10.1002/anie.202004697.
112 K. T. Butler, C. H. Hendon and A. Walsh, *J. Am. Chem. Soc.*, 2014, **136**, 2703–2706.
113 F. M. Ismail, D. O'Neil, T. Youssef and S. A. Elfeky, *J. Energy Chem.*, 2019, **29**, 88–94.
114 J. T. Joyce, F. R. Laffir and C. Silien, *J. Phys. Chem. C*, 2013, **117**, 12502–12509.
115 S. Goswami, L. Ma, A. B. Martinson, M. R. Wasielewski, O. K. Farha and J. T. Hupp, *ACS Appl. Mater. Interfaces*, 2016, **8**, 30863–30870.
116 J. Zhu, W. A. Maza and A. J. Morris, *J. Photochem. Photobiol., A*, 2017, **344**, 64–77.
117 M. Cai, Q. Loague and A. J. Morris, *J. Phys. Chem. Lett.*, 2020, **11**, 702–709.
118 S. Goswami, I. Hod, J. Duan, C.-W. Kung, M. Rimoldi, C. D. Malliakas, R. H. Palmer, O. K. Farha and J. T. Hupp, *J. Am. Chem. Soc.*, 2019, **141**, 17696–17702.

119 D. Van Gough, T. N. Lambert, D. R. Wheeler, M. A. Rodriguez, M. T. Brumbach, M. D. Allendorf and E. D. Spoerke, *ACS Appl. Mater. Interfaces*, 2014, **6**, 1509–1514.
120 M. D. Allendorf, M. E. Foster, F. Leonard, V. Stavila, P. L. Feng, F. P. Doty, K. Leong, E. Y. Ma, S. R. Johnston and A. A. Talin, *J. Phys. Chem. Lett.*, 2015, **6**, 1182–1195.
121 A. M. Ullman, J. W. Brown, M. E. Foster, F. Leonard, K. Leong, V. Stavila and M. D. Allendorf, *Inorg. Chem.*, 2016, **55**, 7233–7249.
122 C. Liu, C. Wang, H. Wang, T. Wang and J. Jiang, *Eur. J. Inorg. Chem.*, 2019, **2019**, 4815–4819.
123 A. A. Talin, A. Centrone, A. C. Ford, M. E. Foster, V. Stavila, P. Haney, R. A. Kinney, V. Szalai, F. El Gabaly, H. P. Yoon, F. Léonard and M. D. Allendorf, *Science*, 2014, **343**, 66–69.
124 J. Liu, T. Wächter, A. Irmler, P. G. Weidler, H. Gliemann, F. Pauly, V. Mugnaini, M. Zharnikov and C. Wöll, *ACS Appl. Mater. Interfaces*, 2015, **7**, 9824–9830.
125 Z. Guo, D. K. Panda, M. A. Gordillo, A. Khatun, H. Wu, W. Zhou and S. Saha, *ACS Appl. Mater. Interfaces*, 2017, **9**, 32413–32417.
126 C. Schneider, D. Ukaj, R. Koerver, A. A. Talin, G. Kieslich, S. P. Pujari, H. Zuilhof, J. Janek, M. D. Allendorf and R. A. Fischer, *Chem. Sci.*, 2018, **9**, 7405–7412.
127 X. Liu, M. Kozlowska, T. Okkali, D. Wagner, T. Higashino, G. Brenner-Weiß, S. M. Marschner, Z. Fu, Q. Zhang, H. Imahori, S. Bräse, W. Wenzel, C. Wöll and L. Heinke, *Angew. Chem., Int. Ed.*, 2019, **58**, 9590–9595.
128 G. O. Ngongang Ndjawa, M. R. Tchalala, O. Shekhah, J. I. Khan, A. E. Mansour, J. Czaban-Jóźwiak, L. J. Weselinski, H. A. Ahsaine, A. Amassian and M. Eddaoudi, *Materials*, 2019, **12**, 2457.
129 F. Rouhani, F. Rafizadeh-Masuleh and A. Morsali, *J. Am. Chem. Soc.*, 2019, **141**, 11173–11182.
130 P. Mani, N. Mandal, M. Roopesh, H. Gopalakrishnan, A. Datta and S. Mandal, *J. Mater. Chem. C*, 2020, **8**, 4836–4842.
131 S. M. Pratik, L. Gagliardi and C. J. Cramer, *J. Phys. Chem. C*, 2020, **124**, 1878–1887.
132 S. M. Pratik, L. Gagliardi and C. J. Cramer, *Chem. Mater.*, 2020, **32**, 6137–6149.
133 K. Leong, M. E. Foster, B. M. Wong, E. D. Spoerke, D. Van Gough, J. C. Deaton and M. D. Allendorf, *J. Mater. Chem. A*, 2014, **2**, 3389–3398.
134 D. Wu, Y. Wang, N. Ma, K. Cao, W. Zhang, J. Chen, D. Wang, Z. Gao, F. Xu and K. Jiang, *Electrochim. Acta*, 2019, **305**, 474–483.
135 L. M. Tijerina, C. M. O. González, B. I. Kharissov, T. E. S. Quezada, Y. P. Méndez, O. V. Kharissova and I. G. de la Fuente, *Mendeleev Commun.*, 2019, **29**, 400–402.